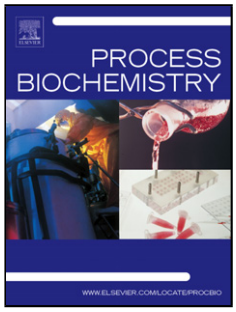

Title: Effect of N/S ratio on anoxic thiosulfate oxidation in a fluidized bed reactor: experimental and artificial neural network model analysis

Authors: Ramita Khanongnuch, Francesco Di Capua, Aino-Maija Lakaniemi, Eldon R. Rene, Piet N.L. Lens

PII: S1359-5113(17)31766-X
DOI: https://doi.org/10.1016/j.procbio.2018.02.018
Reference: PRBI 11276

To appear in: *Process Biochemistry*

Received date: 11-11-2017
Revised date: 12-2-2018
Accepted date: 21-2-2018

Please cite this article as: Khanongnuch Ramita, Di Capua Francesco, Lakaniemi Aino-Maija, Rene Eldon R, Lens Piet N.L.Effect of N/S ratio on anoxic thiosulfate oxidation in a fluidized bed reactor: experimental and artificial neural network model analysis.*Process Biochemistry* https://doi.org/10.1016/j.procbio.2018.02.018

Effect of N/S ratio on anoxic thiosulfate oxidation in a fluidized bed reactor: experimental and artificial neural network model analysis

Ramita Khanongnuch[a, b*], Francesco Di Capua[c, d], Aino-Maija Lakaniemi[a], Eldon R. Rene[b], Piet N. L. Lens[a, b]

[a] Tampere University of Technology, Faculty of Natural Science, Laboratory of Chemistry and Bioengineering, P. O. Box 541, 33101 Tampere, Finland

[b] UNESCO-IHE Institute for Water Education, 2611 AX Delft, The Netherlands

[c] Department of Civil and Mechanical Engineering, University of Cassino and Southern Lazio, 03043 Cassino, Italy

[d] Department of Civil, Architectural and Environmental Engineering, University of Napoli Federico II, 80125 Napoli, Italy

[*]Corresponding author:

Ramita Khanongnuch

Tampere University of Technology, Faculty of Natural Science, Laboratory of Chemistry and Bioengineering, P. O. Box 541, 33101 Tampere, Finland E-mail: ramita.khanongnuch@tut.fi

Graphical Abstract

Graphical abstract

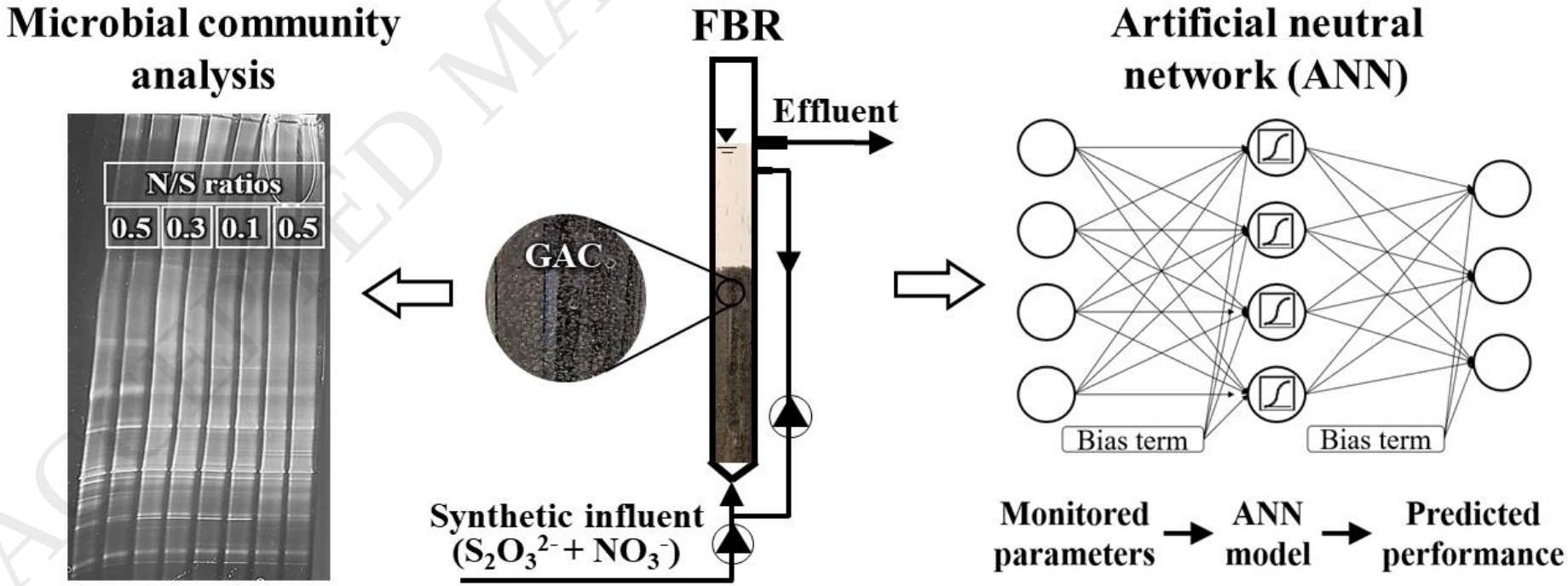

Highlights

- Anoxic $S_2O_3^{2-}$ oxidation in FBR was modelled using artificial neural networks (ANN)
- Sensitivity analysis showed that dissolved oxygen and pH affected $S_2O_3^{2-}$ removal
- *Thiobacillus* sp. dominated the microbial community of the FBR at all N/S ratios
- $S_2O_3^{2-}$ removal efficiency recovered to 80% within 3 days after extreme starvation
- Nitrate starvation detrimentally affected the anoxic $S_2O_3^{2-}$ oxidation kinetics

Abstract

Anoxic thiosulfate ($S_2O_3^{2-}$) oxidation using autotrophic denitrification by a mixed culture of nitrate reducing, sulfur oxidizing bacteria (NR-SOB) was studied in a fluidized bed reactor (FBR). The long-term performance of the FBR was evaluated for 306 days at three nitrogen-to-sulfur (N/S) molar ratios (0.5, 0.3 and 0.1) and a hydraulic retention time (HRT) of 5 h. $S_2O_3^{2-}$ removal efficiencies > 99% were obtained at a N/S ratio of 0.5 and a $S_2O_3^{2-}$ and nitrate (NO_3^-) loading rate of 820 (±84) mg S-$S_2O_3^{2-}$ L^{-1} d^{-1} and 173 (±10) mg N-NO_3^- L^{-1} d^{-1}, respectively. The $S_2O_3^{2-}$ removal efficiency decreased to 76% and 26% at N/S ratios of 0.3 and 0.1, respectively, and recovered to 80% within 3 days after increasing the N/S ratio from 0.1 back to 0.5. The highest observed half-saturation (K_s) and inhibition (K_I) constants of the biofilm-grown NR-SOB obtained from batch cultivations were 172 and 800 mg S-$S_2O_3^{2-}$ L^{-1}, respectively. *Thiobacilus denitrificans* was the dominant microorganism in the FBR. Artificial neural network modelling successfully predicted $S_2O_3^{2-}$ and NO_3^- removal efficiencies and SO_4^{2-} production in the FBR. Additionally, results from the sensitivity

analysis showed that the effluent pH was the most influential parameter affecting the $S_2O_3^{2-}$ removal efficiency.

Keywords: Anoxic thiosulfate oxidation, kinetic constants, nitrate reducing-sulfur oxidizing bacteria, *Thiobacilus denitrificans*, artificial neutral network

1. Introduction

Sulfide compounds (S^{2-}, HS^- and H_2S) present in wastewater and biogas streams, particularly in industrial discharges from fermentation of molasses, pulp and paper industry and latex production, can cause odor and corrosion problems [1,2]. The removal of sulfide from both liquid and gaseous phases has been implemented by various physico-chemical methods, including scrubbing, adsorption, absorption and chemical precipitation [3,4]. However, these technologies have high operating costs as well as negative environmental impacts due to the generation of chemical wastes [4,5].

Biological processes for sulfide removal are considered as cleaner and less expensive alternatives compared to conventional technologies using chemicals. Aerobic and anoxic bioreactors have been operated for sulfide removal from both liquid and gas streams [6–9]. Anoxic bioreactors are more practically applicable than the aerobic ones in terms of ease of use and operational costs [7,10]. Particularly, the use of aerobic bioreactors for biogas cleaning can cause various problems, including the dilution of biogas by oxygen. For safety

reasons, it is also necessary to control the oxygen to methane ratio in order to avoid reaching explosive limits [11].

Different bioreactor configurations have been operated under anoxic conditions for sulfide removal from liquid waste streams. Dolejs *et al*. [12] studied sulfide removal using autotrophic denitrification in a continuous stirred tank reactor (CSTR) and reported that the sulfide removal efficiency decreased from 96% to 55% and the denitrification was completely inhibited when the CSTR was operated at a N/S ratio lower than 0.42. In another study using an activated sludge augmented with *T. denitrificans*, the $S_2O_3^{2-}$ removal efficiency became very unstable when the N/S ratio was decreased from 1.0 to 0.9 [13]. CSTRs are, however, susceptible to biomass wash-out and therefore require a high solid retention time (SRT) resulting in larger reactor volumes than biofilm systems, which can efficiently retain biomass [14,15]. Biofilm systems, e.g. fluidized bed reactors (FBR), have been widely used for sulfide removal under aerobic and micro-aerobic conditions [16-19]. Using oxygen as an electron acceptor can cause the formation of polysulfides as well as mass transfer limitations of oxygen and sulfide to the immobilized biomass [16]. Recently, FBRs have been extensively studied for NO_3^- removal using reduced sulfur compounds as electron donors at different temperatures and pH conditions [20-22].

Nitrate-reducing, sulfide oxidizing bacteria (NR-SOB) such as *Thiobacillus denitrificans* and *Sulfurimonas denitrificans* can oxidize sulfide and other reduced sulfur compounds such as elemental sulfur (S^0) and thiosulfate ($S_2O_3^{2-}$) by using NO_3^- as electron acceptor in the absence of oxygen [13,23]. The stoichiometry of anoxic HS^- and $S_2O_3^{2-}$ oxidation by NR-SOB is represented by the following reactions [24,25]:

$$HS^- + 1.23NO_3^- + 0.573H^+ + 0.027CO_2 + 0.438HCO_3^- + 0.093NH_4^+ \rightarrow SO_4^{2-} + 0.614N_2 + 0.866H_2O + 0.093C_5H_7O_2N \quad (1)$$

$S_2O_3^{2-} + 1.16NO_3^- + 0.124H_2O + 0.035CO_2 + 0.519HCO_3^- + 0.11NH_4^+ \rightarrow 2SO_4^{2-} + 0.578N_2 + 0.435H^+ + 0.110C_5H_7O_2N$ (2)

The application of artificial neural networks (ANNs) for modeling non-linear bioprocesses is effective in evaluating the performance of biological waste-gas treatment systems, particularly biofilters and biotrickling filters [26,27]. Recently, ANNs have been used to predict FBR performance in various applications, i.e. treatment of sulfate-rich wastewaters and heap bioleaching solutions [28-31]. The ANN model was for example successfully applied to predict the removal efficiencies of SO_4^{2-} and COD, and S^{2-} production in a biological SO_4^{2-} reduction process with a network topology of 5-11-3 [29]. The authors also carried out a sensitivity analysis in order to ascertain the relationship between the input parameters and their effects on the outputs, which showed that the influent pH mainly affected the sulfidogenic process.

Previous studies have shown that the nitrogen to sulfur (N/S) ratio is one of the key operational factors for anoxic sulfide-oxidizing bioreactors, since it affects the metabolism of the sulfide-oxidizing bacteria and the ratio of the end-products formed during sulfide oxidation, i.e. S^0 and sulfate (SO_4^{2-}) [9,12,32]. These studies, however, did not test the long-term performance and microbial community evolution under different N/S ratios, neither used ANN modeling to evaluate the performance and relationship of the process variables of anoxic H_2S or $S_2O_3^{2-}$ oxidation. In this study, $S_2O_3^{2-}$ was used as the model sulfur compound for H_2S due to being the first intermediate formed by NR-SOB during H_2S oxidation and its high solubility which is easier to handle in laboratory-scale experiments compared to H_2S [33].

The objective of this study was to evaluate the long-term performance of an FBR for $S_2O_3^{2-}$ oxidation using NO_3^- as the electron acceptor at different N/S ratios (0.5, 0.3 and 0.1) using the following tests: (1) the resilience of the FBR to long-term NO_3^- limiting conditions

by operating at an extreme low N/S ratio (N/S ratio 0.1) for over 40 days; (2) batch activity tests to evaluate the kinetic parameters of the immobilized biomass under steady-state at each studied N/S ratio; (3) polymerase chain reaction-denaturing gradient gel electrophoresis (PCR-DGGE) to study the evolution of the microbial community in the FBR biofilms and (4) ANN modeling to predict the $S_2O_3^{2-}$ and NO_3^- removal efficiencies and SO_4^{2-} concentration in the FBR for $S_2O_3^{2-}$ oxidation, while the modelled data was subjected to a sensitivity analysis to determine the key parameters affecting the $S_2O_3^{2-}$ and NO_3^- removal efficiencies.

2. Materials and methods

2.1. Medium preparation

The mineral medium used in this study was composed of $Na_2S_2O_3$ (470 g L^{-1}), KNO_3, (72-280 g L^{-1}), $NaHCO_3$ (1 g L^{-1}), KH_2PO_4 (2 g L^{-1}), NH_4Cl (1 g L^{-1}), $MgSO_4 \cdot 7H_2O$ (0.8 g L^{-1}), $FeSO_4 \cdot 7H_2O$ (2 g L^{-1}) and 2 mL L^{-1} of a trace element solution as described by Zou *et al*. [20]. The influent pH was adjusted to 7.0 using 37% HCl. All chemicals used in this study were of laboratory grade.

2.2. Experimental set-up and operating conditions

The lab-scale FBR had an empty bed volume of 0.58 L and a height of 40 cm, similar to the configuration described by Zou *et al*. [20]. The reactor was operated at a hydraulic retention time (HRT) of 5 h and at room temperature (20 ± 2 °C). Filtrasorb®200 granular activated carbon (GAC) (Calgon Carbon, USA) was used as the carrier material. The expansion of the reactor bed was maintained at 20-25% of the bed height. The FBR was previously operated for 705 days to study thiosulfate-driven denitrification at different nitrogen loading rates (NLR) [20], pH and temperature [21,22]. The influent tank was connected to a Tedlar gasbag filled with N_2 to prevent oxygen diffusion into the tank and to maintain the dissolved oxygen (DO) concentration as low as possible.

In this study, $S_2O_3^{2-}$ and NO_3^- removal efficiencies were evaluated under three different N/S molar ratios (0.5, 0.3 and 0.1) for 306 days (Table 1). The FBR operation was divided into four experimental periods in which the influent $S_2O_3^{2-}$ concentration was maintained at 200 mg S-$S_2O_3^{2-}$ L^{-1}, whereas the influent NO_3^- concentration was decreased stepwise from 40 mg N-NO_3^- L^{-1} (N/S 0.5, period I) to 20 (N/S 0.3, period II) and 10 mg N-NO_3^- L^{-1} (N/S 0.1, period III), respectively. During period IV, the N/S ratio was increased to 0.5 in order to evaluate the recovery of the $S_2O_3^{2-}$ oxidation efficiency after a 42-day starvation period at a N/S ratio of 0.1. Steady-state conditions in each period of FBR operation were assumed when the relative standard deviation (%RSD) of the $S_2O_3^{2-}$ removal efficiency was < 10%. The loading rate (LR), removal efficiency (RE) and volumetric removal rate (VRR) of $S_2O_3^{2-}$ and NO_3^- in the FBR were estimated using the following equations:

$$LR\ (mg\ L^{-1}d^{-1}) = \frac{C_{in} \times Q}{V} \quad (3)$$

$$RE\ (\%) = \frac{C_{in} - C_{out}}{C_{out}} \times 100 \quad (4)$$

$$VRR\ (\mathrm{g}\ L^{-1}d^{-1}) = LR \times \frac{RE\ (\%)}{100} \quad (5)$$

where C_{in} and C_{out} are influent and effluent concentrations of NO_3^- (mg N-NO_3^- L^{-1}) or $S_2O_3^{2-}$ (mg S-$S_2O_3^{2-}$ L^{-1}), respectively.

Table 1.

2.3. Batch activity tests

Batch activity tests were performed in duplicate in order to measure the specific uptake rate of $S_2O_3^{2-}$ and to determine the affinity of the biomass to $S_2O_3^{2-}$. For each test, 10-mL of biofilm-coated GAC was collected from the FBR during steady-state conditions of experimental periods II, III and IV (on days 196, 244 and 305) and used in three separate batch activity tests (tests A, B and C). A sample of 400 (±50) mg VSS L^{-1} biomass was added to 120 mL serum bottles with 40 mL headspace. The medium used in these batch assays was

the same as in the FBR experiment. The batch bottles were placed on a HS 501 horizontal shaker (IKA, USA) with 220 rpm mixing and maintained at 20 (±2) °C. The initial concentrations of $S_2O_3^{2-}$ and NO_3^- used in the batch activity tests are reported in Table 2. $S_2O_3^{2-}$ oxidation coupled to NO_3^- reduction was described using the Haldane model (Eq. 6). Besides a Haldane term describing the potential substrate inhibition by $S_2O_3^{2-}$, a Michaelis-Menten term was also considered to take into account NO_3^- limitation (Eq. 6).

$$r_S = \frac{r_{max_S} \times S}{K_s + S + \frac{S^2}{K_I}} \times \frac{N}{K_n + N} \quad (6)$$

where S, K_s and K_I are the concentration, half-saturation constant and inhibition constant for $S_2O_3^{2-}$ (mg S L^{-1}), respectively, N and K_n are the concentration and half-saturation constant for NO_3^- (mg N L^{-1}), respectively, and r_{max_S} is the maximum specific uptake rate for $S_2O_3^{2-}$ (mg S g VSS^{-1} h^{-1}).

Table 2.

2.4. Residence time distribution (RTD) test

The RTD test was conducted at the end of the FBR experiments in order to determine the hydrodynamic behavior of the FBR. A tracer, 10-mL of a 1 M KCl solution, was pulse injected into the influent stream. During the test, the conductivity of the effluent was measured using a Multiparameter inoLab Multi Level 1 meter equipped with a KLE 325 probe (WTW, Germany). In order to validate the RTD test, two flow rates of 360 and 108 mL h^{-1} were applied. The hydrodynamic behavior of the FBR was determined using Eqs. 7-9. The Morrill Dispersion Index (MDI) (Eq. 10) was used to evaluate the flow characteristics in the FBR.

$$\text{RTD function } (E(t)) = \frac{C_i}{\sum C_i \Delta t_i} \quad (7)$$

$$\text{Mean residence time } (t_m) = \frac{\sum t_i C_i \Delta t_i}{\sum C_i \Delta t_i} \quad (8)$$

$$\text{Experimental amount of outlet tracer} = \sum C_i \Delta t_i \quad (9)$$

$$\text{MDI} = \frac{t_{90}}{t_{10}} \quad (10)$$

where C_i is KCl concentration in the effluent (mg L^{-1}), t_i is the measuring time (h), t_{90} and t_{10} are times when 90% and 10% of the tracer passes through the FBR, respectively.

2.5. Analytical techniques

The liquid samples collected from the FBR and batch bottles were filtered through 0.45 µm Chromafil Xtra PET-202125 membrane syringe filters (Mechery-Nagel, Germany) prior to the measurement of nitrite (NO_2^-), NO_3^-, $S_2O_3^{2-}$ and SO_4^{2-} concentrations by ion chromatography (IC) as described by Di Capua *et al*. [21]. The total dissolved sulfide in the FBR effluent was measured using the Cord-Ruwisch method [34]. The pH of the FBR influent and effluent was measured using a pH 3110 portable meter fitted with a SenTix 21 electrode (WTW, Germany). The DO concentration was measured directly in the FBR using a HQ40d portable multimeter equipped with an Intellical™ LDO101 probe (HACH, USA). Alkalinity and volatile suspended solid (VSS) concentrations of the FBR biofilm were measured according to the procedures described in Standard Methods [35]. To prepare the biomass for the VSS measurement, two samples of 1 mL GAC were mixed in a 15 mL Falcon tube with deionized (DI) water to detach the biofilm from GAC by manual shaking. Subsequently, the liquid portion containing the detached biomass was used to measure the VSS concentration. This procedure was repeated until all biofilm was detached from the GAC based on visual observation.

The concentration of S^0 in the biofilm-coated GAC was estimated by modified cyanolysis [36]. Deionized water containing the cells detached from 1 mL of GAC by manual shaking was mixed with 10 mL of acetone. 200 µL of the obtained solution was mixed with 100 µL of 100 mM KCN and incubated at room temperature (20 ± 2 °C) for 10 min. After incubation, 500 µL of PO_4^{3-} buffer solution (containing 50 ml of 0.2 M NaH_2PO_4 and 39 ml of 0.2 M NaOH) and 100 µL of 1.5 M $Fe(NO_3)_3$ in 4 M $HClO_4$ were added to the mixture.

After centrifugation for 1 min at 14,000 rpm, the optical density (OD) of the supernatant was measured using a UV-1601 spectrophotometer (Shimadzu, Japan) at a wavelength of 460 nm.

2.6. Microbial community analysis

The microbial community of the FBR biofilm was analysed by polymerase chain reaction denaturing gradient gel electrophoresis (PCR-DGGE) followed by sequencing. Two samples of 1 mL of biofilm-coated GAC were collected from the FBR during steady-state operations of each experimental period (days 114, 196, 242 and 306), and sonicated for 2 min in sterile de-ionized water to detach all the bacterial cells from the carrier material. The solution containing the microorganisms was filtered through a Cyclopore track etched 0.2 µm membrane (Whatman, USA), and the biomass samples collected on the filters were stored at -20 ºC for further analysis.

DNA was extracted from the defrosted filters using a PowerSoil® DNA isolation kit (MO BIO Laboratories, Inc., USA) according to the manufacturer's instructions. A primer pair Bac357F-GC and Un907R was used for amplifying the partial bacterial 16S rRNA genes by using a T3000 thermalcycler (Biometra, Germany) as described by Kolehmainen *et al*. [37]. DGGE was performed with a INGENY phorU2 × 2 - system (Ingeny International BV, GV Goes, The Netherlands) as reported by Kolehmainen *et al*. [37]. The amplified samples were sequenced by Macrogen (South Korea). The obtained sequences were analyzed using the Bioedit software (version 7.2.5, Ibis Biosciences, USA) and compared with the sequences available at the National Center for Biotechnology Information (NCBI) database (http://blast.ncbi.nlm.nih.gov).

2.7. ANN model development

The ANN modeling was performed using the Neural Net Fitting application in the Neural Network Toolbox 11.0 of MATLAB® R2017b (MathWorks Inc., USA). The multilayer perceptron described in Fig. 1 was a feed-forward network in which the neurons in the input

layer received the normalized input signals and passed those signals to the hidden layer after multiplying them with the respective connection weights. A tan-sigmoidal transfer function was used in the hidden layer, while a linear (PURELIN) transfer function was used in the output layer, respectively.

The inputs to the ANN model consisted of pH, DO, influent concentrations of $S_2O_3^{2-}$ ($S_2O_3^{2-}{}_{in}$) and NO_3^- ($NO_3^-{}_{in}$), respectively, while the ANN outputs were $S_2O_3^{2-}$ ($S_2O_3^{2-}$-RE) and NO_3^- (NO_3^--RE) removal efficiencies and SO_4^{2-} production ($SO_4^{2-}{}_{ef}$), respectively. Table 3 shows the basic statistics of the training, validation and test data used to develop the ANN model. In order to suit the transfer function and avoid outliers, the raw input and output data were normalized to the range of 0-1, according to Eq. 11. The experimental data (days 45-306) was randomly divided into training (70%), validation (10%) and testing (20%) sample sets.

The ANN was trained using the Levenberg-Marquardt back-propagation algorithm (trainlm function), while the mean squared error (MSE) and regression analysis were used for estimating the error between the model fitted and the experimental data. The strength of the relationship between the output and input variables was evaluated by sensitivity analysis, which was performed using the shareware version of the multivariable statistical modelling software, NNMODEL (PA, USA).

$$\hat{X} = \frac{X - X_{min}}{X_{max} - X_{min}} \quad (11)$$

where $\hat{X}$ is the normalized value, X_{min} and X_{max} are the minimum and maximum values of X, respectively.

Fig. 1.

Table 3.

2.8. Data analysis

The statistical analysis of the data was performed using the Minitab 16 software. The one-way analysis of variance (ANOVA) was conducted in order to compare the pH, DO, $S_2O_3^{2-}$ and NO_3^- concentrations and the respective removal efficiencies and SO_4^{2-} production at the steady-state of each operational period. The significant level was set at 95% ($P \leq 0.05$). To determine the kinetic parameters, the Haldane equation (Eq. 6) was applied using the non-linear programming solver (fminsearch) in MATLAB® R2017b (MathWorks Inc., USA) in order to optimize the experimental data using r_{max_S}, K_S, K_I and K_n as the optimization variables.

3. Results

3.1. FBR performance

Fig. 2 shows the profiles of effluent pH, NO_3^-, NO_2^-, $S_2O_3^{2-}$, SO_4^{2-} and DO concentration during the 306 days of operation. The influent pH was maintained at 6.9 (±0.1). The consumed N/S ratio slightly fluctuated but remained close to 0.5, while the alkalinity consumption varied in the range of 25 to 145 mg HCO_3^- L^{-1} during the entire FBR operation. NO_2^- was never detected in the effluent during the study. During the entire experiment, the VSS concentration of the FBR biofilm was relatively constant, being 21.7 (±4.9) g VSS L^{-1} of GAC, based on measurements conducted on days 0, 60, 114, 196, 242 and 306. S^0 was visually observed on the GAC carrier as white particles and its concentration showed an increasing trend as the feed N/S ratios were deceased. The measured S^0 concentration of the biofilm-coated GAC was approximately 9, 13 and 26 mg L^{-1} on days 200, 240 and 300, respectively.

During period I (N/S ratio of 0.5), the loading rates of $S_2O_3^{2-}$ and NO_3^- were 820 (±84) mg S-$S_2O_3^{2-}$ L^{-1} d^{-1} and 173 (±10) mg N-NO_3^- L^{-1} d^{-1}, respectively. During the first 38 days of operation, the concentrations of $S_2O_3^{2-}$, SO_4^{2-} and DO in the FBR effluent were not stable

(Fig. 2). Therefore, the DO concentration in the reactor was decreased from 0.43 (±0.07) (days 0-38) to 0.25 (±0.05) (days 39-306) mg L^{-1} by connecting a N_2 gasbag to the influent tank. During steady-state operation of period I (days 101-115), $S_2O_3^{2-}$ and NO_3^- removal efficiencies were 99% and 100%, respectively, with SO_4^{2-} as the main end-product. The volumetric removal rate of $S_2O_3^{2-}$ was 810 (±80) g $S\text{-}S_2O_3^{2-}$ L^{-1} d^{-1} and the effluent SO_4^{2-} concentration was 740 (±60) mg L^{-1}, 35% higher than the theoretical value in period I (550 mg L^{-1}) calculated according to Eq. 2. The effluent pH during period I was 6.8 (±0.2).

During periods II (N/S ratio 0.3) and III (N/S ratio 0.1), the feed NO_3^- loading rate was decreased from 175 (period I) to 125 and 50 g $N\text{-}NO_3^-$ L^{-1} d^{-1}, respectively (Table 1). NO_3^- was completely consumed in both periods II and III, whereas the $S_2O_3^{2-}$ removal efficiency decreased to 76% in period II and further to 26% in period III (under steady-state operation), resulting in effluent SO_4^{2-} concentrations of 580 (±30) and 200 (±15) mg L^{-1}, respectively. The effluent pH gradually increased from 6.8 (±0.2) (period I) to 7.1 (±0.1) and 7.3 (±0.1) in periods II and III, respectively. During period III (N/S ratio 0.1), biofilm detachment from the GAC was also visually observed.

During period IV, the N/S ratio was increased to 0.5 as in period I. As a result, the $S_2O_3^{2-}$ removal efficiency increased from 26% in period III to 80% in period IV in 3 days. Although the $S_2O_3^{2-}$ removal efficiency in period IV was 20% lower than in period I, the SO_4^{2-} concentration in the effluent (680 ± 60 mg L^{-1}) was only 8% lower than in period I. During period IV, the effluent pH was 7.2 (±0.1), higher than the one measured at the same N/S ratio in period I.

Fig. 2.

3.2. Batch activity tests

Fig. 3 shows the maximum specific uptake rate, half-saturation and inhibition constants for $S_2O_3^{2-}$ (r_{max}, K_s and K_I, respectively) estimated from the batch activity tests A, B and C

(Table 2). The highest half-saturation constant, K_n, for NO_3^- reduction was 6.32 mg N-NO_3^- L^{-1} and was obtained with the NR-SOB cultivated during period IV (N/S ratio of 0.5). The biomass taken during period III (N/S ratio 0.1) showed the lowest K_I for $S_2O_3^{2-}$ oxidation, while it was the highest with the biomass taken at a N/S ratio of 0.5 (period IV). The $S_2O_3^{2-}$ removal efficiencies obtained in tests A, B and C were 84.5 (±12.8)%, 26.3 (±3.5)% and 91.6 (±8.4)%, respectively (data not shown). NO_2^- was found as an intermediate of the process, but no NO_2^- was detected at the end of the batch activity tests (data not shown).

Fig. 3.

3.3. Hydrodynamic flow characteristics of the FBR

The RTD curves of the FBR at the flow rates of 360 and 108 mL h^{-1} are shown in Fig. 4. The mass recovery of KCl used as a tracer was 90%. Most of the tracer was washed out within 1 and 2 h at flow rates of 360 and 108 mL h^{-1}, respectively, while the rest of the tracer was slowly removed (Fig. 4). The results obtained from the RTD curves indicated that the effective mean residence time in the FBR at flow rates of 360 and 108 mL h^{-1} were 2.1 and 6.7 h, respectively. The computed MDI values (MDI = 9 and 11) for the two flow rates described the hydraulic regime in the FBR as semi-complete mixing. In the case of an effective plug flow, the MDI has a value of 2 or less, whereas the value for a completely mixed system is 22 [38].

Fig. 4.

3.4. Microbial community profiling in the FBR

The microbial community profiles of the FBR biofilm during periods I, II, III and IV showed that operation at different N/S ratios resulted in changes in the microbial community composition (Fig. 5). Based on the affiliations of the nucleotide sequences obtained from the BLAST analysis, 8 of the 15 sequenced bands were identified as known facultative autotrophic sulfide-oxidizing bacteria (Table 4, bands 1, 6-10, 12 and 13). The closest

relatives of the known bacteria were *T. denitrificans* (band 8, 99% similarity) and *T. thioparus* (bands 6 and 7, 92-99.8% similarity). Bands 1 and 9 were also detected as a *Thiobacillus* genus; however, the sequence results were shown as uncultured representative of the genus with no species-level information. During period IV (N/S ratio 0.5), the band representing *T. denitrificans* (band 8) faded away and was replaced by bands identified as *T. thioparus* (bands 6 and 7). The band associated to *Thiomonas* sp. (band 13) and uncultured *Sulfuritalea* (band 12) showed a higher intensity at N/S ratios of 0.3 and 0.1 than at a N/S ratio of 0.5. The chemo-organotrophic *Flavobacteriaceae* (bands 2 and 3), *Chryseobacterium* sp. (band 4) and *Simplicispira* sp. (band 10) were detected at all N/S ratios tested. Additionally, *Desulfovibrio* sp. (band 14), a SO_4^{2-} reducing bacterium, was detected in the FBR biofilm throughout the entire experiment.

Fig. 5.

Table 4.

3.5. ANN modeling

Fig. 6 shows the experimentally verified and ANN predicted profiles of the $S_2O_3^{2-}$ and NO_3^- removal efficiencies and SO_4^{2-} concentration. The network topology was obtained at the following settings of the internal network parameters: learning rate (1.0) and epoch size (10). The performance of the Levenberg-Marquardt back-propagation algorithm was achieved with a MSE of 0.006523, while the determination coefficient (R^2) of the training, validation, test and overall predicted data were 0.90, 0.95, 0.88 and 0.90, respectively. At the best network topology for the FBR as 4-4-3, the connection weights and the bias terms were obtained for the interconnections between the neurons in different layers of the multilayer perceptron (Table 5).

Fig. 6.

Table 5.

The sensitivity analysis of the ANN model was represented in terms of the absolute average sensitivity (AAS) and the average sensitivity (AS), as shown in Table 6. Table 6 shows that the removal efficiency of $S_2O_3^{2-}$ was affected by the effluent pH and DO concentrations with AAS values of 0.53 and 0.24, respectively. The removal efficiency of NO_3^- was affected by the influent $S_2O_3^{2-}$ and NO_3^- concentrations with AAS values of 0.54 and 0.36, respectively. Besides, the SO_4^{2-} production depended on the $S_2O_3^{2-}$ and DO concentrations.

Table 6.

4. Discussion

4.1. Effect of NO_3^- limitation on FBR performance

This study showed that NO_3^- dosing can be used to remove sulfur compounds, i.e. $S_2O_3^{2-}$ as model for H_2S, from waste or scrubbing wasters. The NR-SOB in the FBR showed high stability to $S_2O_3^{2-}$ oxidation at all N/S ratios tested, evidenced by the comparison between the fed and consumed N/S ratios during the entire experiment (Table 1). The consumed N/S ratio was close to 0.5 during periods I, II and III, while it slightly increased close to 0.6 during period IV (Table 1). During the latter period, the $S_2O_3^{2-}$ removal efficiency of the FBR decreased because NO_3^- was completely depleted over time (Fig. 2).

The FBR showed high robustness and resiliency since the $S_2O_3^{2-}$ oxidation efficiency rapidly recovered after operating under extreme nitrate-limiting conditions (period III), i.e. N/S ratio 0.1 compared to the stoichiometric requirement of N/S ratio 0.6 as shown as Eq. 2 (Fig. 2). Starvation periods have often been applied to test the robustness and resilience of bioreactors. Chen *et al*. [39] applied a H_2S starvation period of 15 days in a two-layer biotrickling filter (BTF), observing an increase in H_2S removal efficiency from 65% to 99% during the 4 days starvation period. Recently, *Thiobacillus*-dominated FBR biofilms have shown extremely high sulfur oxidation and NO_3^- reduction rates even under extreme

operational conditions, such as low temperature (< 5°C) [21], low pH of 5.0 [22] and high heavy metal concentrations, i.e. 20-100 mg Ni L^{-1} [40] or 86.6 mg Co L^{-1} [41]. The high biomass concentrations of the FBR biofilm (Table 7) likely played an important role in providing resistance to substrate fluctuations during this study. However, the $S_2O_3^{2-}$ removal efficiency during period IV (N/S ratio 0.1) was about 20% lower than in period I at the same N/S ratio. The lower $S_2O_3^{2-}$ removal efficiencies observed during period IV could be attributed to the changes in the microbial community of the FBR biofilm, particularly *T. denitrificans* was absent (below detection limit of DGGE) in period IV (Fig. 5, Table 4).

Table 7.

In this study, SO_4^{2-} was the main product of $S_2O_3^{2-}$ oxidation (Fig. 2). The reduction of 1 g of N-NO_3^- under $S_2O_3^{2-}$ oxidation produced 19.4 (±1.8) g of SO_4^{2-} in the FBR effluent, which is 31% higher than the theoretical value of 11.8 g of SO_4^{2-} calculated according to Eq. 2. The excess of SO_4^{2-} in the FBR effluent could be attributed to two mechanisms. The facultative anaerobic sulfur oxidizing bacteria, i.e. *Thiobacillus* sp. and *Thiomonas* sp., populating the FBR biofilm can also use oxygen as electron acceptor to oxidize the S^0 accumulated in the bioreactor during previous operation [20,22]. Alternatively, the unexpectedly high SO_4^{2-} concentrations in the effluent could be due to sulfur disproportionation under anoxic conditions, which occurs as described by Eq. 12 [43]:

$$4S^0 + 4H_2O \rightarrow 3H_2S + SO_4^{2-} + 2H^+ \quad (12)$$

During this study, S^0 was also measured and visually observed as white particles attached on the GAC carrier material of the FBR. Previous studies have reported the accumulation of S^0 during S^{2-} and $S_2O_3^{2-}$ oxidation both in bioreactors [12,32] and batch bioassays [42] as a result of electron donor overloading or NO_3^- starvation [24]. Besides, Sahinkaya et al. [44] reported that low NO_3^- loading rates could promote biological sulfur disproportionation in anoxic reactor columns packed with S^0.

The biofilm detachment from the GAC in the FBR observed from period III onwards likely occurred as a response to NO_3^- starvation. Under this condition, the deeper biofilm layer experiences a lack of substrate that can lead to biofilm detachment and after a more extended period to reactor failure [14]. However, wash-out of suspended cells was minimal as the VSS concentration was relatively stable (21.7 ± 4.9 g VSS L^{-1} of GAC) during the entire experiment.

4.2. Effect of NO_3^- starvation on the microbial community of the FBR biofilm

The microbial community composition of the FBR biofilm changed during FBR operation at different N/S ratios (Fig. 5). Sulfur-oxidizing bacteria of the genus *Thiobacillus* were found as the dominant microorganisms in the FBR biofilm during the whole operation (Table 4) and were mainly responsible for NO_3^- consumption. In particular, *T. denitrificans* (band 8) has a good ability to be immobilized with other microorganisms promoting biofilm formation [45]. *T. thioparus* (bands 6-7) can reduce NO_3^- using $S_2O_3^{2-}$ as electron donor and has been reported to be less sensitive to high $S_2O_3^{2-}$ concentrations than *T. denitrificans* [23]. DGGE profiling (Fig. 5) showed that long-term NO_3^- starvation favoured *T. thioparus* over *T. denitrificans*.

During period IV, *T. thioparus* (band 6 and 7) outgrew both *T. denitrificans* (band 8) and *Thiomonas* sp. (band 13). This may also explain the lower $S_2O_3^{2-}$ consumption in period IV compared to period I, since *T. thioparus* can use $S_2O_3^{2-}$ only to reduce NO_3^- to NO_2^- [45]. NO_2^- was, nevertheless, never detected in the FBR effluent, and it was presumably consumed by other denitrifying bacteria (e.g. band 11) present in the FBR biofilm.

Despite the presence of *Desulfovobrio sp.* in the microbial community of the FBR biofilm, SO_4^{2-} reduction rates were almost negligible, probably due to the lack of external electron donors. This was also confirmed by the observed SO_4^{2-} concentration in the effluent which was higher than the theoretical value, confirming that SO_4^{2-} consumption did not occur

in this study. It is also possible that some other denitrifying bacteria were playing a role in the nitrogen bioconversion in the FBR, but were present in concentrations below the detection limit of the PCR-DGGE.

4.3. Effect of N/S ratio on the $S_2O_3^{2-}$ oxidation kinetics based on batch bioassays

The highest affinity constant, K_s value of 171.9 mg L^{-1} obtained at a N/S ratio of 0.1 (Table 2), indicates a low $S_2O_3^{2-}$ oxidation activity by the NR-SOB populating the FBR biofilm at extreme nitrate-limiting conditions. The K_s values estimated at N/S ratios of 0.3 and 0.5 (Table 2) were closer to the values reported by Mora et al. [46] (16.1 mg S-$S_2O_3^{2-}$ L^{-1}) for a suspended culture of thiosulfate-oxidizing denitrifiers at a N/S ratio of 1.3. Biofilm cultures of NR-SOB have higher K_s values compared to suspended-growth cultures [44] as a result of diffusion limitations of the substrates within the biofilm [47].

The lowest value of the inhibition constant K_I (200 mg $S_2O_3^{2-}$ L^{-1}) was obtained at a N/S ratio of 0.1, indicating that substrate inhibition by $S_2O_3^{2-}$ occurred at the highest $S_2O_3^{2-}$ concentration tested in the batch bioassays (Table 2, Fig. 3). Substrate inhibition by $S_2O_3^{2-}$ was also observed in previous studies performing batch tests with both suspended [48] and biofilm [23] cultures of NR-SOB at concentrations exceeding 2.2 g S-$S_2O_3^{2-}$ L^{-1}. However, the results of this study (Table 2) showed that $S_2O_3^{2-}$ can also inhibit NR-SOB activity at lower concentrations, i.e. 800 mg S-$S_2O_3^{2-}$ L^{-1}.

4.4. ANN modeling and sensitivity analysis

The AAS and AS values could be used to identify the most influential input parameters (pH, DO, $NO_{3\,in}^{-}$ and $S_2O_{3\,in}^{2-}$) affecting the FBR performance [49], i.e. $S_2O_3^{2-}$ and NO_3^- removal efficiency as well as SO_4^{2-} production. According to the removal of sulfur compounds in anoxic FBRs, the change in input parameters could have significant impact on the overall bioreactor performance [18,20,21]. The ANN model was able to provide adequate information in the form of a contour plot to reveal the effects of different operational

conditions on the FBR performance (Fig. 7). Accordingly, the influent NO_3^- concentration should be > 100 mg NO_3^- L^{-1} in order to achieve $S_2O_3^{2-}$ removal efficiencies > 80%, and the effluent pH should be maintained at values > 4.0. This observation is strongly supported by the experimental results of this study in which the effluent pH during the entire experiment was higher than 7.0 (Fig. 2). Besides, a previously operated FBR wherein the thiosulfate-driven NO_3^- removal was achieved at a pH of 4.8 to 6.9, resulting in an increase in the removal efficiency at higher pH values [22]. The sensitivity analysis results also revealed that the DO concentrations strongly affected both the $S_2O_3^{2-}$ removal efficiency (AS = -0.24) and effluent SO_4^{2-} concentrations (AS = -0.36). These results from the sensitivity analysis were in good agreement with the experimental result obtained during days 0-38, which showed that a high DO concentration led to fluctuations in $S_2O_3^{2-}$ removal efficiency (Fig. 2).

Fig. 7.

4.5. Practical implications: use of NO_3^- dosing for sulfide removal

For full scale operation, the FBR can be considered as a reliable technology to scale-up for the removal of $S_2O_3^{2-}$ and other sulfur compounds (e.g. HS^- and S^{2-}) under anaerobic conditions, e.g. using NO_3^- as the electron acceptor. Long-term reactor operation can lead to unexpected events, such as substrate starvation, which can dramatically reduce the bioreactor performance. The FBR used in this study demonstrated good robustness and resilience, particularly, the FBR was able to recover 80% of the initial $S_2O_3^{2-}$ removal efficiency within 3 days following starvation (period III, N/S ratio 0.1). However, changes in the microbial community of the FBR biofilm during the starvation period may affect the sulfide oxidation rates and must thus be avoided in practice.

In full-scale, wastewater and wastegas treatment systems are usually controlled with online monitoring equipment, such as programmable sensors which can be integrated with the ANN model in order to control and predict the reactor performance [26]. The results from

the ANN modeling associated with the sensitivity analysis obtained from this study (Fig. 6) suggest that ANN can be used offline for monitoring and assessing the performance of full-scale FBR using autotrophic denitrification treating wastewater containing both $S_2O_3^{2-}$ and NO_3^-, e.g. mining or $H_2S/S_2O_3^{2-}$ containing scrubbing liquors used for treating H_2S contaminated gases.

5. Conclusions

High (99%) $S_2O_3^{2-}$ removal efficiencies were obtained in a FBR using NO_3^- as electron acceptor using the following parameters: N/S ratio of 0.5, 20 ºC, HRT of 5 h and influent pH of 6.9 (±0.1). Batch activity tests indicated that decreasing the N/S ratio resulted in increasing the biomass affinity constant, K_S, and decreasing the inhibition constant, K_I, of the NR-SOB immobilized in the FBR. The $S_2O_3^{2-}$ oxidation efficiency in the FBR recovered to 80% within 3 days following an increase in N/S ratio to 0.5 after a 42-day starvation period (N/S of 0.1). *Thiobacillus* sp. was the dominant microorganism in the FBR biofilm and primarily responsible for $S_2O_3^{2-}$ oxidation using NO_3^- as electron acceptor. The ANN model successfully predicted the performance parameters of the FBR, i.e. $S_2O_3^{2-}$ and NO_3^- removal efficiency and effluent SO_4^{2-} concentration. The sensitivity analysis results showed that effluent pH was the most influential parameter affecting the $S_2O_3^{2-}$ removal efficiency. Besides, the influent $S_2O_3^{2-}$ concentration affected the NO_3^- removal efficiency and the effluent SO_4^{2-} concentration.

Acknowledgements

This research was supported by the European Union's Horizon 2020 research and innovation programme under the Marie Skłodowska-Curie grant agreement no. 643071.

References

[1] L. Guerrero, S. Montalvo, C. Huiliñir, J.L. Campos, A. Barahona, R. Borja, Advances in the biological removal of sulphides from aqueous phase in anaerobic processes: a

review, Environ. Rev. 24 (2015) 84-100. doi:10.1139/er-2015-0046.

[2] C. Rattanapan, P. Boonsawang, D. Kantachote, Removal of H_2S in down-flow GAC biofiltration using sulfide oxidizing bacteria from concentrated latex wastewater, Bioresour. Technol. 100 (2009) 125-130. doi:10.1016/j.biortech.2008.05.049.

[3] A.H. Nielsen, P. Lens, J. Vollertsen, T. Hvitved-Jacobsen, Sulfide-iron interactions in domestic wastewater from a gravity sewer, Water Res. 39 (2005) 2747-2755. doi:10.1016/j.watres.2005.04.048.

[4] R. Muñoz, L. Meier, I. Diaz, D. Jeison, A review on the state-of-the-art of physical/chemical and biological technologies for biogas upgrading, Rev. Environ. Sci. Biotechnol. 14 (2015) 727-759. doi:10.1007/s11157-015-9379-1.

[5] N. Abatzoglou, S. Boivin, A review of biogas purification processes, Biofuels, Bioprod. Biorefin. 3 (2009) 42-71. doi:10.1002/bbb.117.

[6] Q. Mahmood, P. Zheng, J. Cai, D. Wu, B. Hu, J. Li, Anoxic sulfide biooxidation using nitrite as electron acceptor, J. Hazard. Mater. 147 (2007) 249-256. doi: 10.1016/j.jhazmat.2007.01.002.

[7] F. Almenglo, M. Ramírez, J.M. Gómez, D. Cantero, Operational conditions for start-up and nitrate-feeding in an anoxic biotrickling filtration process at pilot scale, Chem. Eng. J. 285 (2016) 83-91. doi:10.1016/j.cej.2015.09.094.

[8] E. Can-Dogan, M. Turker, L. Dagasan, A. Arslan, Sulfide removal from industrial wastewaters by lithotrophic denitrification using nitrate as an electron acceptor, Water Sci. Technol. 62 (2010) 2286-2293. doi:10.2166/wst.2010.545.

[9] A. Bayrakdar, E. Tilahun, B. Calli, Biogas desulfurization using autotrophic denitrification process, Appl. Microbiol. Biotechnol. 100 (2016) 939-948. doi:10.1007/s00253-015-7017-z.

[10] M. Fernández, M. Ramírez, J.M. Gómez, D. Cantero, Biogas biodesulfurization in an

anoxic biotrickling filter packed with open-pore polyurethane foam, J. Hazard. Mater. 264 (2014) 529-535. doi:10.1016/j.jhazmat.2013.10.046.

[11] M. Fernández, M. Ramírez, R.M. Pérez, J.M. Gómez, D. Cantero, Hydrogen sulphide removal from biogas by an anoxic biotrickling filter packed with Pall rings, Chem. Eng. J. 225 (2013) 456-463. doi:10.1016/j.cej.2013.04.020.

[12] P. Dolejs, L. Paclík, J. Maca, D. Pokorna, J. Zabranska, J. Bartacek, Effect of S/N ratio on sulfide removal by autotrophic denitrification, Appl. Microbiol. Biotechnol. 99 (2015) 2383-2392. doi:10.1007/s00253-014-6140-6.

[13] I. Manconi, A. Carucci, P. Lens, Combined removal of sulfur compounds and nitrate by autotrophic denitrification in bioaugmented activated sludge system, Biotechnol. Bioeng. 98 (2007) 551-560. doi:10.1002/bit.21383.

[14] S. Papirio, D.K. Villa-Gomez, G. Esposito, F. Pirozzi, P.N.L. Lens, Acid mine drainage treatment in fluidized-bed bioreactors by sulfate-reducing bacteria: a critical review, Crit. Rev. Environ. Sci. Technol. 43 (2013) 2545-2580. doi:10.1080/10643389.2012.694328.

[15] F. Di Capua, S. Papirio, P.N.L. Lens, G. Esposito, Chemolithotrophic denitrification in biofilm reactors, Chem. Eng. J. 280 (2015) 643-657. doi:10.1016/j.cej.2015.05.131.

[16] B. Krishnakumar, S. Majumdar, V.B. Manilal, A. Haridas, Treatment of sulphide containing wastewater with sulphur recovery in a novel reverse fluidized loop reactor (RFLR), Water Res. 39 (2005) 639-647. doi:10.1016/j.watres.2004.11.015.

[17] L. Krayzelova, J. Bartacek, I. Díaz, D. Jeison, E.I.P. Volcke, P. Jenicek, Microaeration for hydrogen sulfide removal during anaerobic treatment: a review, Rev. Environ. Sci. Biotechnol. 14 (2015) 703-735. doi:10.1007/s11157-015-9386-2.

[18] A.P. Annachhatre, S. Suktrakoolvait, Biological sulfide oxidation in a fluidized bed reactor, Env. Technol. 22 (2001) 661-672. doi:10.1080/09593332208618238.

[19] V. Midha, M.K. Jha, A. Dey, Sulfide oxidation in fluidized bed bioreactor using nylon support material, J. Environ. Sci. 24 (2012) 512-519. doi:10.1016/S1001-0742(11)60799-7.

[20] G. Zou, S. Papirio, A-M. Lakaniemi, S.H. Ahoranta, J.A. Puhakka, High rate autotrophic denitrification in fluidized-bed biofilm reactors, Chem. Eng. J. 284 (2016) 1287-1294. doi:10.1016/j.cej.2015.09.074.

[21] F. Di Capua, I. Milone, A-M. Lakaniemi, P.N.L. Lens, G. Esposito, High-rate autotrophic denitrification in a fluidized-bed reactor at psychrophilic temperatures, Chem. Eng. J. 313 (2017) 591-598. doi:10.1016/j.cej.2016.12.106.

[22] F. Di Capua, A-M. Lakaniemi, J.A. Puhakka, P.N.L. Lens, G. Esposito, High-rate thiosulfate-driven denitrification at pH lower than 5 in fluidized-bed reactor, Chem. Eng. J. 310 (2017) 282-291. doi:10.1016/j.cej.2016.10.117.

[23] F. Di Capua, S.H. Ahoranta, S. Papirio, P.N.L. Lens, G. Esposito, Impacts of sulfur source and temperature on sulfur-driven denitrification by pure and mixed cultures of *Thiobacillus*, Process Biochem. 51 (2016) 1576-1584. doi:10.1016/j.procbio.2016.06.010.

[24] M. Mora, M. Fernández, J.M. Gómez, D. Cantero, J. Lafuente, X. Gamisans, D. Gabriel, Kinetic and stoichiometric characterization of anoxic sulfide oxidation by SO-NR mixed cultures from anoxic biotrickling filters, Appl. Microbiol. Biotechnol. 99 (2014) 77-87. doi:10.1007/s00253-014-5688-5.

[25] M. Mora, L.R. López, X. Gamisans, D. Gabriel, Coupling respirometry and titrimetry for the characterization of the biological activity of a SO-NR consortium, Chem. Eng. J. 251 (2014) 111-115. doi:10.1016/j.cej.2014.04.024.

[26] E.R. Rene, M.E. López, M.C. Veiga, C. Kennes, Neural network models for biological waste-gas treatment systems, N. Biotechnol. 29 (2011) 56-73.

doi:10.1016/j.nbt.2011.07.001.

[27] V. V. Nair, H. Dhar, S. Kumar, A.K. Thalla, S. Mukherjee, J.W.C. Wong, Artificial neural network based modeling to evaluate methane yield from biogas in a laboratory-scale anaerobic bioreactor, Bioresour. Technol. 217 (2016) 90-99. doi:10.1016/j.biortech.2016.03.046.

[28] S. Janyasuthiwong, E.R. Rene, G. Esposito, P.N.L. Lens, Effect of pH on the performance of sulfate and thiosulfate-fed sulfate reducing inverse fluidized bed reactors, J. Environ. Eng. 142 (2016). doi:10.1061/(ASCE)EE.1943-7870.0001004.

[29] L.C. Reyes-Alvarado, N.N. Okpalanze, D. Kankanala, E.R. Rene, G. Esposito, P.N.L. Lens, Forecasting the effect of feast and famine conditions on biological sulphate reduction in an anaerobic inverse fluidized bed reactor using artificial neural networks, Process Biochem. 55 (2017) 146-161. doi:10.1016/j.procbio.2017.01.021.

[30] B. Ozkaya, E. Sahinkaya, P. Nurmi, A.H. Kaksonen, J.A. Puhakka, Biologically Fe^{2+} oxidizing fluidized bed reactor performance and controlling of Fe^{3+} recycle during heap bioleaching: an artificial neural network-based model, Bioprocess Biosyst. Eng. 31 (2008) 111-117. doi:10.1007/s00449-007-0153-9.

[31] V. Midha, M.K. Jha, A. Dey, Neural network prediction of fluidized bed bioreactor performance for sulfide oxidation, Korean J. Chem. Eng. 30 (2013) 385-391. doi:10.1007/s11814-012-0128-7.

[32] B.S. Moraes, T.S.O. Souza, E. Foresti, Effect of sulfide concentration on autotrophic denitrification from nitrate and nitrite in vertical fixed-bed reactors, Process Biochem. 47 (2012) 1395-1401. doi:10.1016/j.procbio.2012.05.008.

[33] M. Mora, A. Guisasola, X. Gamisans, D. Gabriel, Examining thiosulfate-driven autotrophic denitrification through respirometry, Chemosphere. 113 (2014) 1–8. doi:10.1016/j.chemosphere.2014.03.083.

[34] R. Cord-Ruwisch, A quick method for the determination of dissolved and precipitated sulfides in cultures of sulphate-reducing bacteria., J. Microbiol. Methods. 4 (1985) 33-36. doi:10.1016/0167-7012(85)90005-3.

[35] American Public Health Association (APHA), American Water Works Association (AWWA), Water Environment Federation (WEF), Standard methods for the examination of water and wastewater, 20th ed., APHA, AWWA, WEF, Washington D.C., 1999.

[36] D.P. Kelly, A.P. Wood, Reclassification of some species of *Thiobacillus* to the newly designated genera *Acidithiobacillus* gen. nov., *Halothiobacillus* gen. nov. and *Thermithiobacillus* gen. nov., Int. J. Syst. Evol. Microbiol. 50 (2000) 511-516. doi:10.1099/00207713-50-2-511.

[37] R.E. Kolehmainen, J.H. Langwaldt, J.A. Puhakka, Natural organic matter (NOM) removal and structural changes in the bacterial community during artificial groundwater recharge with humic lake water, Water Res. 41 (2007) 2715-2725. doi:10.1016/j.watres.2007.02.042.

[38] Metcalf & Eddy Inc., G. Tchobanoglous, H.D. Stensel, R. Tsuchihashi, F.L. Burton, Wastewater engineering: treatment and resource recovery, 5th ed., McGraw-Hill Education, New York, 2014.

[39] Y. Chen, X. Wang, S. He, S. Zhu, S. Shen, The performance of a two-layer biotrickling filter filled with new mixed packing materials for the removal of H_2S from air, J. Environ. Manage. 165 (2016) 11-16. doi:10.1016/j.jenvman.2015.09.008.

[40] F. Di Capua, I. Milone, A-M. Lakaniemi, E.D. van Hullebusch, P.N.L. Lens, G. Esposito, Effects of different nickel species on autotrophic denitrification driven by thiosulfate in batch tests and a fluidized-bed reactor, Bioresour. Technol. 238 (2017) 534-541. doi:10.1016/j.biortech.2017.04.082.

[41] G. Zou, S. Papirio, A. Ylinen, F. Di Capua, A.M. Lakaniemi, J.A. Puhakka, Fluidized-bed denitrification for mine waters. Part II: effects of Ni and Co, Biodegradation. 25 (2014) 417-423. doi:10.1007/s10532-013-9670-1.

[42] R. Beristain-Cardoso, R. Sierra-Alvarez, P. Rowlette, E.R. Flores, J. Gómez, J.A. Field, Sulfide oxidation under chemolithoautotrophic denitrifying conditions, Biotechnol. Bioeng. 95 (2006) 1148-1157. doi:10.1002/bit.21084.

[43] K. Finster, W. Liesack, B. Thamdrup, Elemental sulfur and thiosulfate disproportionation by *Desulfocapsa sulfoexigens* sp. nov., a new anaerobic bacterium isolated from marine surface sediment, Appl. Environ. Microbiol. 64 (1998) 119-125.

[44] E. Sahinkaya, N. Dursun, A. Kilic, S. Demirel, S. Uyanik, O. Cinar, Simultaneous heterotrophic and sulfur-oxidizing autotrophic denitrification process for drinking water treatment: control of sulfate production, Water Res. 45 (2011) 6661-6667. doi:10.1016/j.watres.2011.09.056.

[45] D. Pokorna, J. Zabranska, Sulfur-oxidizing bacteria in environmental technology, Biotechnol. Adv. 33 (2015) 1246-1259. doi:10.1016/j.biotechadv.2015.02.007.

[46] M. Mora, A.D. Dorado, X. Gamisans, D. Gabriel, Investigating the kinetics of autotrophic denitrification with thiosulfate: modeling the denitritation mechanisms and the effect of the acclimation of SO-NR cultures to nitrite, Chem. Eng. J. 262 (2015) 235-241. doi:10.1016/j.cej.2014.09.101.

[47] R. Sierra-Alvarez, R. Beristain-Cardoso, M. Salazar, J. Gómez, E. Razo-Flores, J.A. Field, Chemolithotrophic denitrification with elemental sulfur for groundwater treatment, Water Res. 41 (2007) 1253-1262. doi:10.1016/j.watres.2006.12.039.

[48] J.L. Campos, S. Carvalho, R. Portela, A. Mosquera-Corral, R. Méndez, Kinetics of denitrification using sulphur compounds: effects of S/N ratio, endogenous and exogenous compounds, Bioresour. Technol. 99 (2008) 1293-1299.

doi:10.1016/j.biortech.2007.02.007.

[49] E.R. Rene, M.C. Veiga, C. Kennes, Experimental and neural model analysis of styrene removal from polluted air in a biofilter, J. Chem. Technol. Biotechnol. 84 (2009) 941-948. doi:10.1002/jctb.2130.

[50] W. Yang, H. Lu, S.K. Khanal, Q. Zhao, L. Meng, G.H. Chen, Granulation of sulfur-oxidizing bacteria for autotrophic denitrification, Water Res. 104 (2016) 507-519. doi:10.1016/j.watres.2016.08.049.

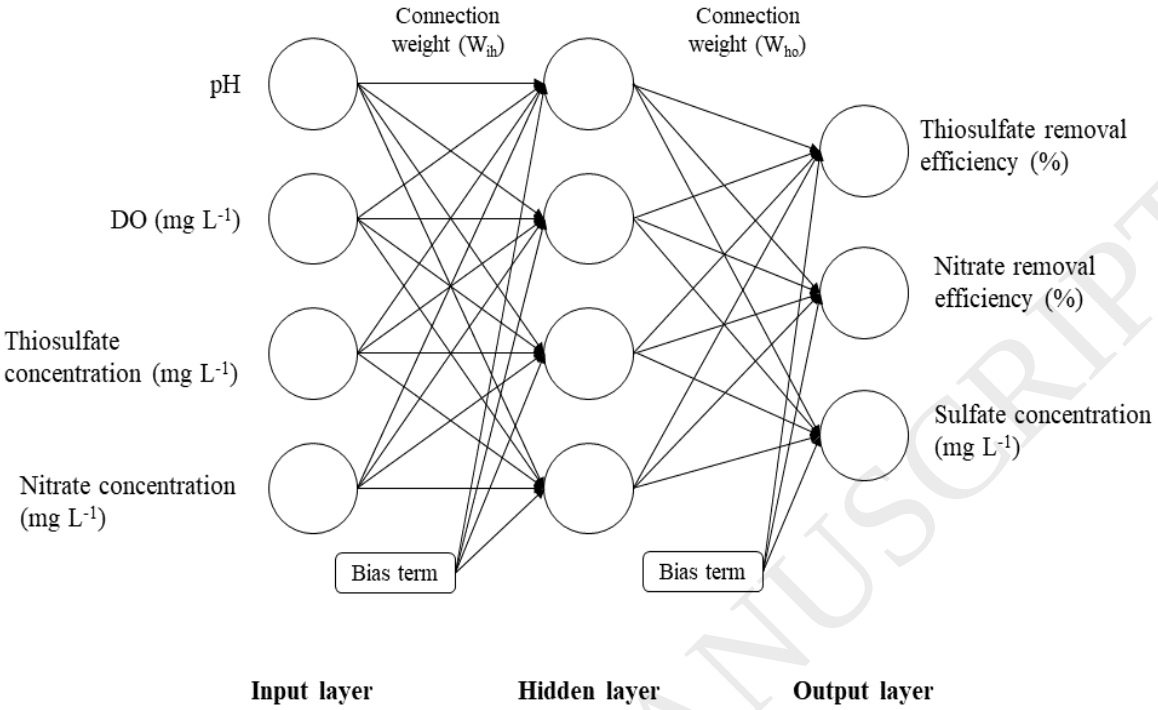

Fig. 1. Architecture of a multilayer perceptron used for predicting the fluidized bed reactor performance by artificial neural network (input-hidden-output = 4-4-3)

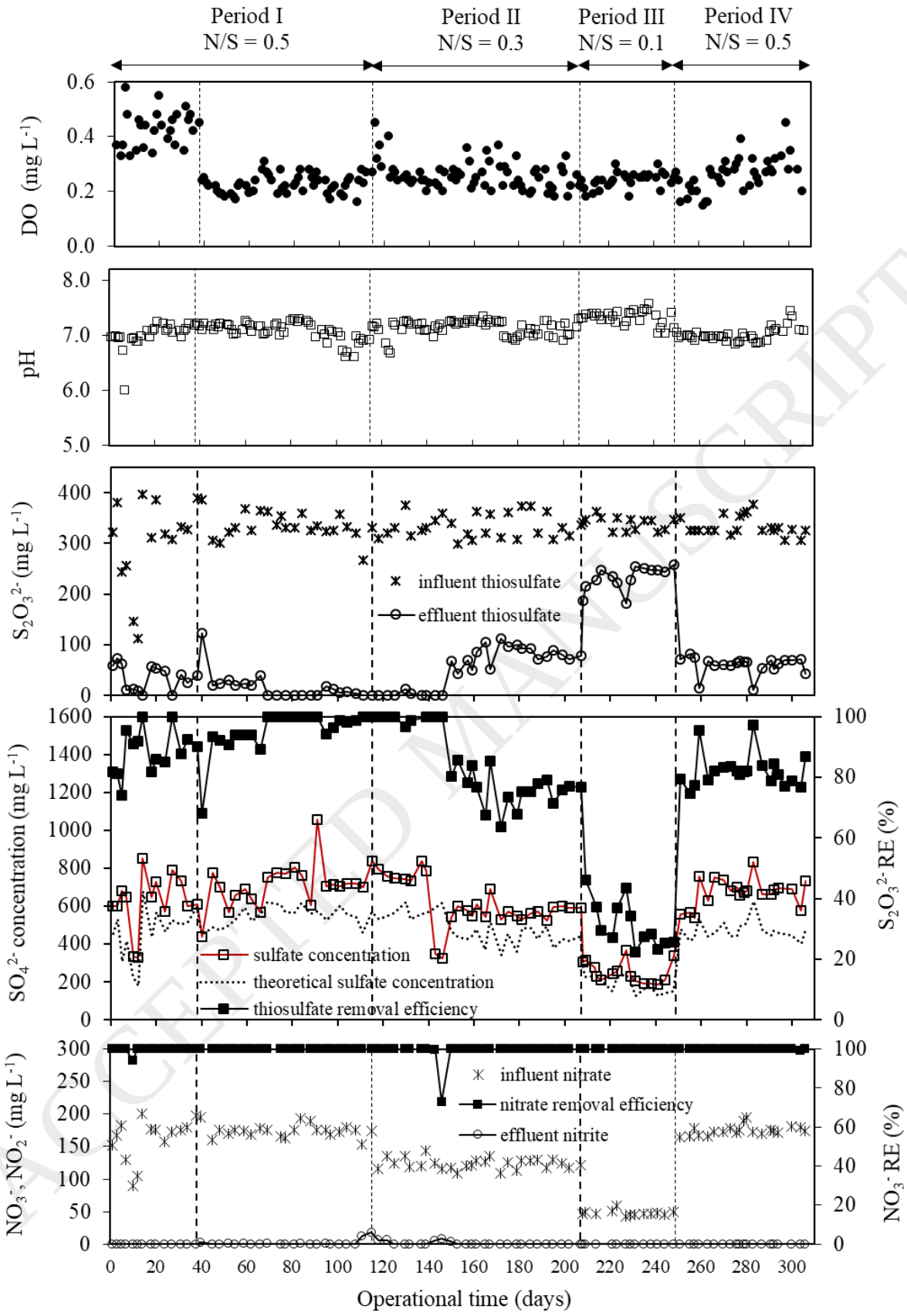

Fig. 2. Time course profiles of dissolved oxygen, pH, $S_2O_3^{2-}$ removal efficiency (RE) in the fluidized bed reactor and influent and effluent concentrations of NO_3^-, NO_2^- and SO_4^{2-}

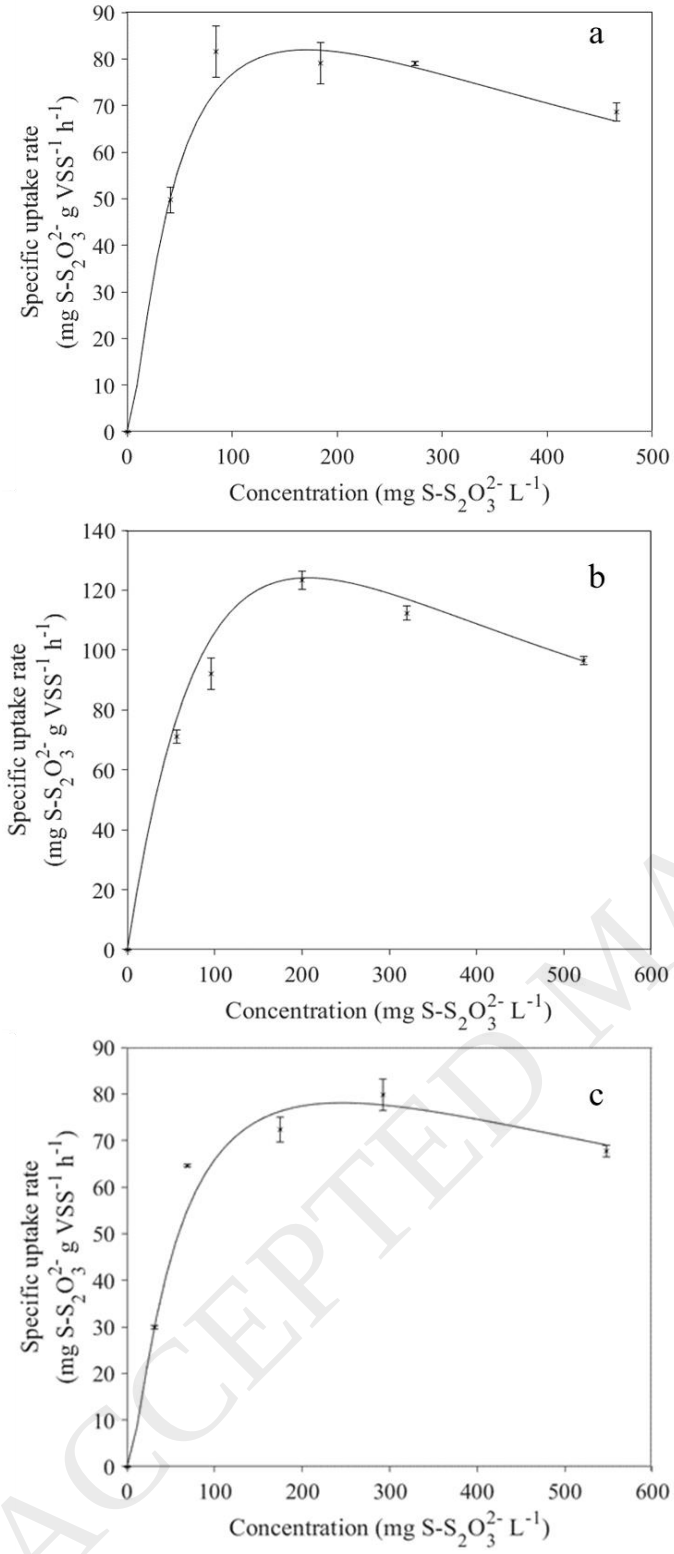

Fig. 3. Haldane plots of thiosulfate uptake rate from batch activity tests at different N/S ratios: (a) 0.3, (b) 0.1 and (c) 0.5. Dots and lines represent experimental and model fitted data, respectively. The error bars indicated the standard error between the experimental and model fitted data

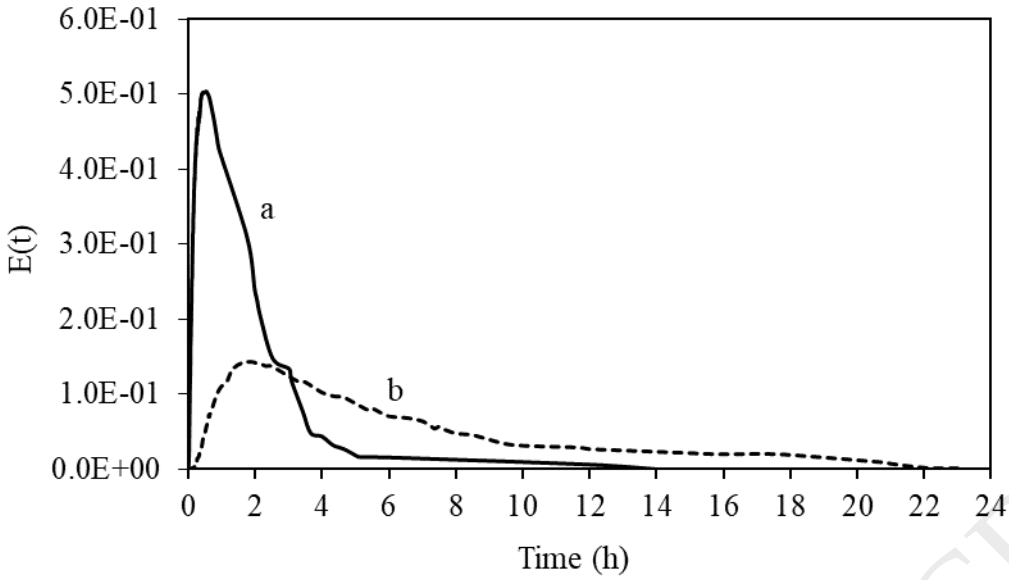

Fig. 4. The residence time distribution (RTD) curves for the FBR at flow rates of (a) 360 and (b) 108 mL h^{-1}

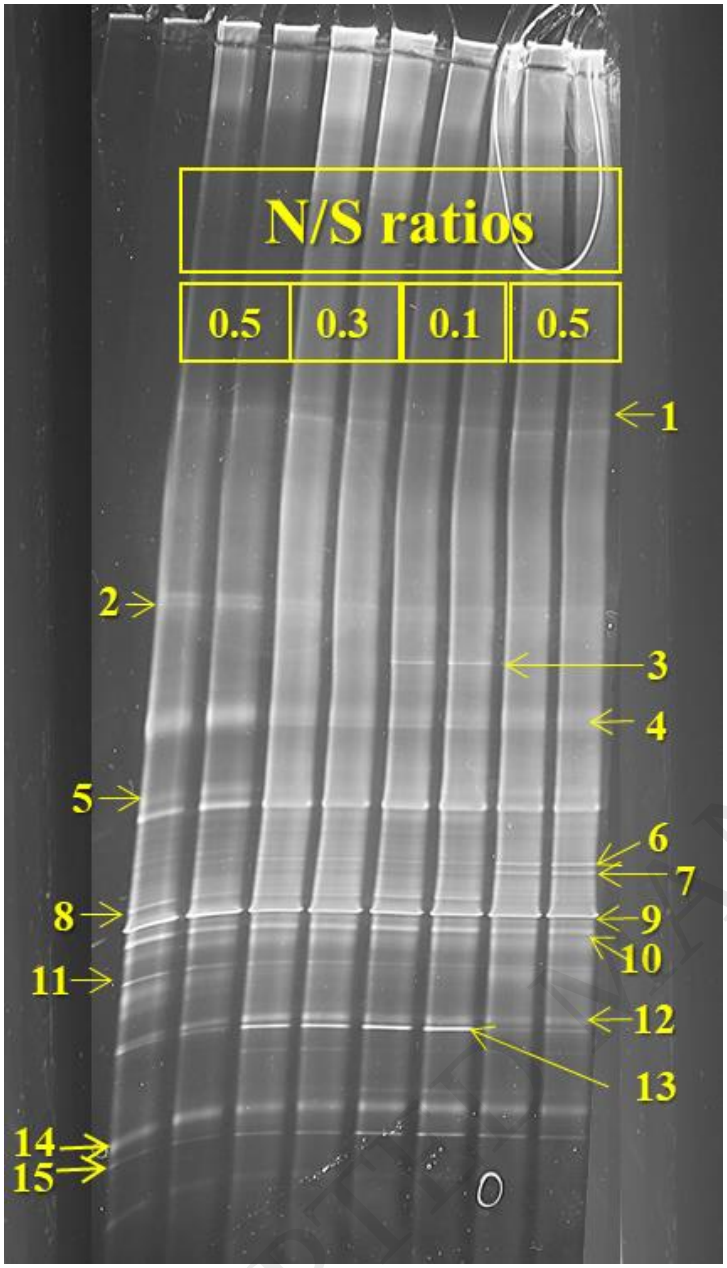

Fig. 5. Microbial community profiling of the fluidized bed reactor biofilm at different N/S ratios. Two duplicate samples were analyzed from each operational period. The affiliations of the bands are given in Table 3

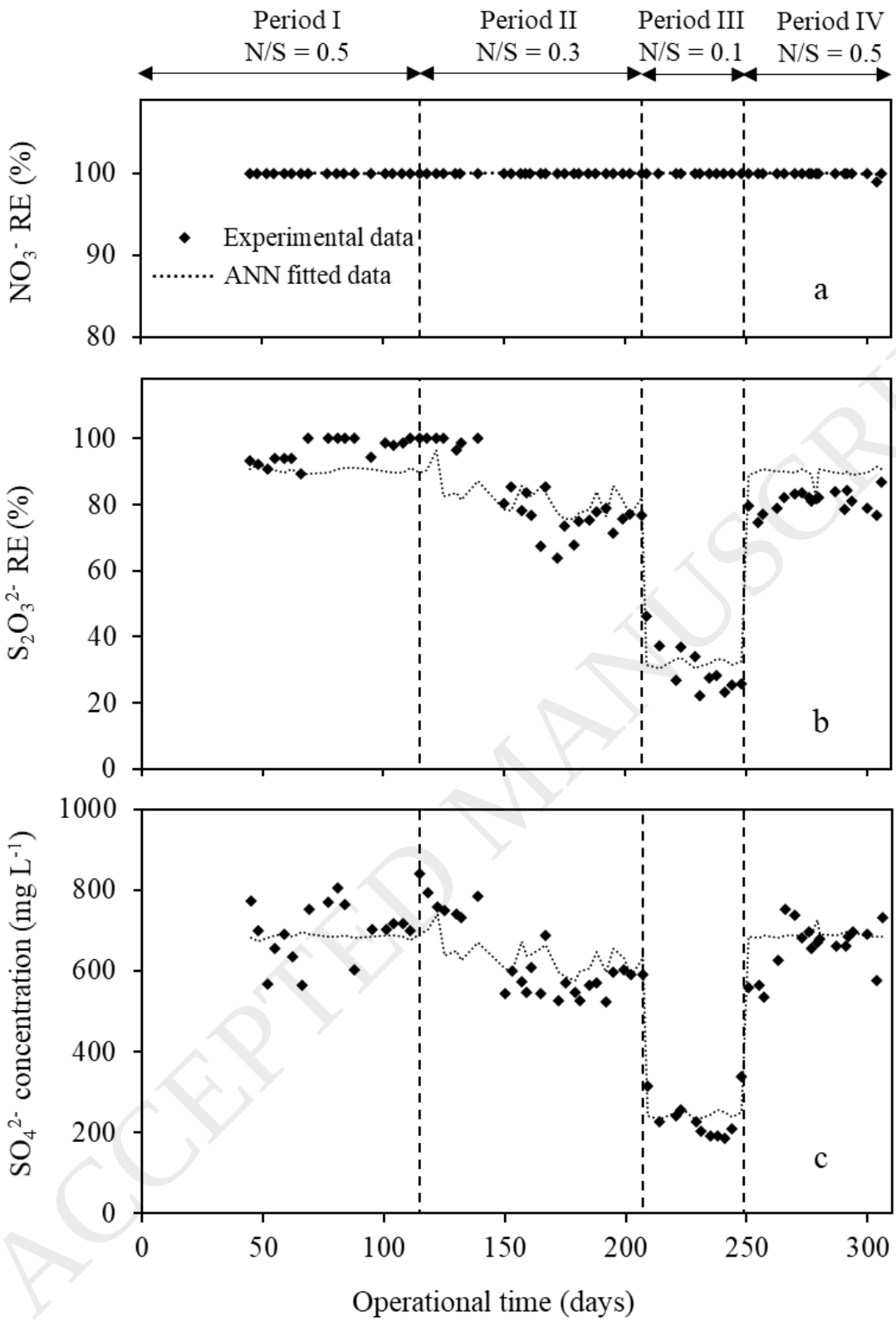

Fig. 6. ANN model fitted data for (a) NO_3^- and (b) $S_2O_3^{2-}$ removal efficiency and (c) SO_4^{2-} concentration in the effluent. Dots and lines represent experimental and predicted model data, respectively

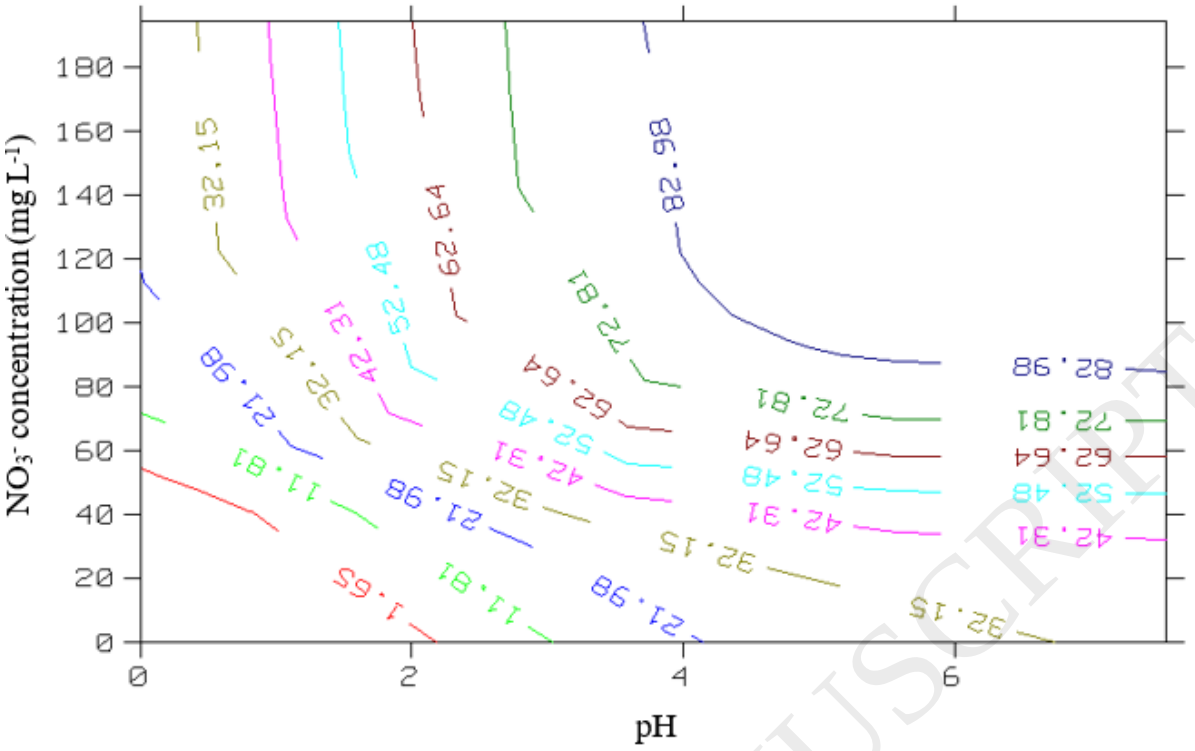

Fig. 7. Contour plot showing the effect of effluent pH and influent NO_3^- concentration on the artificial neural network model predicted $S_2O_3^{2-}$ removal efficiency

Tables

Table 1. Operational conditions and performance of the FBR during the four operation periods

Parameters	**Period I**	**Period II**	**Period III**	**Period IV**
Steady-state duration (days)	101-115	188-207	235-249	292-306
Effluent pH	6.84 ± 0.16	7.11 ± 0.05	7.30 ± 0.05	7.18 ± 0.05
Influent $N\text{-}NO_3^-$ (mg L^{-1})	38.7 ± 10	27.9 ± 1.3	10.7 ± 0.4	39.8 ± 0.8
$N\text{-}NO_3^-$ loading (mg L^{-1} d^{-1})	173 ± 10	125 ± 6	48 ± 2	178 ± 7
$N\text{-}NO_3^-$ removal efficiency (%)	100	100	100	100
Influent $S\text{-}S_2O_3^{2-}$ (mg L^{-1})	184 ± 19	188 ± 11	193 ± 7	183 ± 7
$S\text{-}S_2O_3^{2-}$ loading (mg L^{-1} d^{-1})	822 ± 84	836 ± 54	862 ± 30	817 ± 29
$S\text{-}S_2O_3^{2-}$ removal rate (mg L^{-1} d^{-1})	814 ± 80	642 ± 55	187 ± 94	660 ± 52
$S\text{-}S_2O_3^{2-}$ removal efficiency (%)	99.1 ± 0.9	76.3 ± 2.7	26.0 ± 2.0	80.8 ± 4.1
$S\text{-}SO_4^{2-}$ concentration in the effluent (mg L^{-1})	245 ± 19	192 ± 10	74 ± 22	225 ± 20
Influent N/S ratio	0.49 ± 0.03	0.34 ± 0.03	0.13 ± 0.00	0.50 ± 0.02
Consumed N/S ratio	0.49 ± 0.03	0.45 ± 0.05	0.49 ± 0.06	0.62 ± 0.06

Table 2. Experimental conditions of batch activity tests and the obtained Haldane kinetic coefficients of the nitrate reducing, sulfide oxidizing bacteria taken from the FBR at different N/S ratios

		Initial concentration		**Kinetic coefficients**			
Test	N/S ratio	$S_2O_3^{2-}$ (mg S-$S_2O_3^{2-}$ L^{-1})	NO_3^- (mg N-NO_3^- L^{-1})	r_{max} (mg S-$S_2O_3^{2-}$ g^{-1} VSS h^{-1})	K_S (mg S-$S_2O_3^{2-}$ L^{-1})	K_I (mg S-$S_2O_3^{2-}$ L^{-1})	K_n (mg N-NO_3^- L^{-1})
I	0.3	50, 90 180, 200, 300, 550	7, 14, 30, 45, 65	145.8	21.8	466.1	4.53
II	0.1	50, 90, 200, 300, 550	2, 4, 8, 12, 25	331.3	171.9	247.7	0.25
III	0.5	50, 90, 200, 300, 550	9, 20, 40, 70, 160	127.0	45.1	798.6	6.32

Table 3. Basic statistics of the training, validation and test data used to develop the artificial neural network model

	Mean	**Minimum**	**Maximum**
Dissolved oxygen in the FBR	0.25	0.16	0.40
pH	7.13	6.60	7.57
Influent $S_2O_3^{2-}$ concentration, $S_2O_3^{2-}{}_{in}$ (mg L^{-1})	333.52	267.50	374.94
Influent NO_3^- concentration, $NO_3^-{}_{in}$ (mg L^{-1})	138.02	44.88	194.30
$S_2O_3^{2-}$ removal efficiency, $S_2O_3^{2-}$-RE (%)	77.35	22.25	100.00
NO_3^- removal efficiency, NO_3^--RE (%)	99.99	99.00	100.00
Effluent SO_4^{2-} concentration, $SO_4^{2-}{}_{ef}$ (mg L^{-1})	591.44	186.48	839.48

Table 4. Identification of the microorganisms in the FBR biofilm based on the denaturing gradient gel electrophoresis band sequences (16S rDNA)

Band label	**Affiliation (sequence ID)**	**Matching length**	**Similarity (%)**	**Bacterial class**
1	Uncultured *Thiobacilus* sp. (FJ933304.1)	425	92.0	β-Proteobacteria
2, 3	Uncultured *Flavobacteriaceae* bacterium (EU642061.1)	433-434	91.3-99.3	Flavobacteriales
4	Uncultured *Chryseobacterium* sp. (JQ724349.1)	437	99.3	Flavobacteriales
5	Uncultured bacterium partial 16S rRNA gene, isolate EFW618 (LN889996.1)	463	96.1	
6, 7	*Thiobacillus thioparus* (HM535225.1)	456-474	99.4-99.8	β-Proteobacteria
8	*Thiobacillus denitrificans* (*NR_025358.1*)	431	99.1	β-Proteobacteria
9	Uncultured *Thiobacilus* sp. (KM200026.1)	451-453	99.1-99.8	β-Proteobacteria
10	*Simplicispira* sp. *Iso11-01 gene* (AB795522.1)	437	98.6	β-Proteobacteria
11	Denitrifying bacterium (Y09967.1)	407	93.9	β-Proteobacteria
12	Uncultured *sulfuritalea* (JX493272.1)		97.6	β-Proteobacteria
13	*Thiomonas* sp. (LN864654.1)	467	98.9	β-Proteobacteria
14	*Desulfovibrio* sp. (JX828422.1)	429	99.3	δ-Proteobacteria
15	Uncultured *bacterium clone QKAB4ZG071* (KJ707249.1)	404	94.8	

Table 5. Connection weights between the input → hidden layers (W_{ih}), and the hidden → output layers (W_{ho}) of the artificial neural network model

Model input	**Input → hidden layers (W_{ih})**				**Hidden → output layers (W_{ho})**			
	HID-1	HID-2	HID-3	HID-4		NO_3^--RE	$S_2O_3^{2-}$-RE	$SO_4^{2-}{}_{ef}$
DO	-1.3883	1.9379	-0.0189	-0.35864	HID-1	0.39572	0.42553	-0.12227
pH	-0.75667	-0.05606	0.48028	0.60495	HID-2	-0.34833	0.74721	0.52792
$S_2O_3^{2-}{}_{in}$	-0.31489	-1.2136	-0.24311	-0.79393	HID-3	0.00334	0.82527	0.76574
$NO_3^-{}_{in}$	-0.50078	-0.6068	2.2425	1.3638	HID-4	-0.63191	0.16955	-0.24917
Bias term	2.3203	-2.2994	0.69113	-2.5176	Bias term	-0.3693	0.4252	0.2072

Table 6. Sensitivity analysis of artificial neural network model inputs

Model inputs	**NO_3^--RE (%)**		**$S_2O_3^{2-}$-RE (%)**		**$SO_4^{2-}{}_{ef}$ (mg L^{-1})**	
	AAS	AS	AAS	AS	AAS	AS
DO (mg L^{-1})	0.0758	+0.0758	0.2377	-0.2377	0.3606	-0.3606
pH	0.0290	+0.0290	0.5311	-0.5311	0.1167	+0.1167
$S_2O_3^{2-}{}_{in}$ (mg L^{-1})	0.5369	+0.5369	0.1456	-0.1456	0.359	+0.3590
$NO_3^-{}_{in}$ (mg L^{-1})	0.3583	-0.3583	0.0855	-0.0855	0.1637	-0.1637

Note: RE = removal efficiency, AAS and AS = absolute average sensitivity and average sensitivity, respectively

Type of reactor	**Reactor volume, L**	**Microorganisms**	**Biomass concentration**	**Substrate**	**Feed S-compounds**	**S removal rate**	**N loading rate (mg N-NO_3^- L^{-1} d^{-1})**	**Operational N/S ratios (mol mol^{-1})**	**HRT (h)**	**References**
GSAD	30	Mixed culture of autotrophic & heterotrophic denitrifying bacteria	7 g VSS L^{-1}	Dissolved sulfide (TDS)	100-150 mg S-TDS L^{-1}	0.18 - 0.63 (g S L^{-1} d^{-1})	90-330	0.5-0.7	5-20	[50]
CSTR	2	Mixed culture containing *T. denitrificans*	0.5-0.85 g VSS L^{-1}	$S_2O_3^{2-}$ & S^{2-}	150-570 mg S-$S_2O_3^{2-}$ L^{-1} & 96-125 mg S^{2-} L^{-1}	N.A.	150-500	0.5-1.0	12-20	[13]
CSTR	4	Activated sludge from a municipal treatment plant	0.6 g VSS L^{-1}	S^{2-}	18-176 mg S^{2-} L^{-1}	N.A.	29 -63	0.2-2.4	40	[12]
FBR	0.58	Mix culture of autotrophic denitrifying bacteria	20-28 g VSS L^{-1} of carrier	$S_2O_3^{2-}$	190 mg S-$S_2O_3^{2-}$ L^{-1}	0.2 - 0.8 (g S-$S_2O_3^{2-}$ L^{-1} d^{-1})	50-180	0.1-0.5	5	This study

Table 7. Comparative analysis of various bioreactors performing sulfide or thiosulfate oxidation using autotrophic denitrification

Note: GSAD = granular sludge autotrophic denitrification, N.A. = data not available, CSTR = continuous stirred tank reactor, FBR = fluidized bed reactor, TDS = total dissolved sulfide, S = sulfur, N = nitrogen